Highly Efficient, High-Gain, Short-Length, and Power-Scalable Incoherent Diode Slab-Pumped Fiber Amplifier/Laser

Dmitrii Kouznetsov and Jerome V. Moloney

***Abstract*—We propose a new geometry of a clad-pumped fiber amplifier/laser that includes at least one doped core which guides the signal wave and at least one clad region that guides the incoherent pump. Our proposed geometry enables the incoherent diode pump light to be efficiently absorbed by the doped glass core over very short lengths on the order of a few to tens of centimeters. The transparent cladding is realized as a narrow slab with refractive index higher than that of the core. The slab is designed to effectively capture all of the incoherent pump light and is tapered to force the highly moded incoherent guided light into the strongly absorbing core. Modes of this composite waveguide structure are analyzed in this paper. Criteria are established in terms of the refractive indices of the core, slab, and cladding that ensure efficient absorption of the pump light in the core while ensuring that only a single or few lowest order signal modes can propagate in the amplifying core. Numerical simulations with the beam propagation method and a modal expansion technique confirm that a significant enhancement of the absorption efficiency of the pump in the core can be realized by tapering the slab waveguide. Assuming a local absorption rate of 10 $\mathbf{m}^{-1}$ of the intensity of the pump in a core of radius 4.3 μm and a realistic multimode diode pump distributed over a 100-μm aperture, an absorption efficiency of 94% can be realized over an amplifier length of 2 cm. The geometry is scalable to longer lengths and multiple incoherent diode-pumped slab claddings.**

***Index Terms*—Double-clad (DC) fiber, optical fiber amplifiers, optical fiber lasers.**

I. Introduction

DIODE-BAR pumped double-clad (DC) fiber amplifiers and lasers have been proposed and demonstrated as high-brightness sources capable of delivering 100 W or more of quasi-CW light [1]–[6]. These devices are pumped with multi-watt incoherent diode bars and convert, with high efficiency, incoherent low-brightness light into an almost single transverse-mode high-power output. Attempts to combine multiple high-power fiber lasers to produce powers approaching 1 kW have shown considerable progress of late. The DC fiber geometry is designed to capture a large fraction of the incoherent multi-watt output from the diode bars. A large inner cladding with transversal size ranging from 200 to 300 μm is required to effectively capture the incoherent pump light. The cross section of a conventional DC fiber is shown in Fig. 1(a). Symmetric DC fibers display poor coupling and the core is typically displaced from an axis of symmetry. The absorption of the pump can be characterized by a filling factor F that specifies how much of the pump is localized in the core [7]. However, some modes of the pump are absorbed more efficiently than others [8]–[11] so that F depends on the length of propagation. For an incoherent incident pump field that uniformly fills the inner cladding (ergodic mixing), $F = A_{\rm core}/A_{\rm total}$ where $A_{\rm core}$ is the cross-sectional area of the core and $A_{\rm total}$ is the total cross-sectional area including core and inner cladding. Under these circumstances, we can assume a translational symmetry along the fiber and derive the following estimate for the pump absorption efficiency η:

$$\eta = 1 - \exp(-\alpha F z). \tag{1}$$

In this expression, α refers to the local pump absorption rate and z is the coordinate in the propagation direction. The pump saturation does not modify conclusions regarding optimal inner-cladding/core geometries appropriate for maximum absorption efficiency [12]. So, in this paper, we suppose that α is constant. It should be emphasized that (1) can also offer a reliable estimate for rectangular fibers and circular inner claddings with an offset core. For example, all curves shown in [13, Fig. 7(b)], which is generated by computationally intensive ray-tracing techniques, can be accurately fitted by (1) with the filling factor $F = GA_{\rm core}/A_{\rm total}$ for rectangular cladding and $F = G^2 A_{\rm core}/A_{\rm total}$ for circular offset cladding, where $G = \Gamma(4/3) \approx .89$ and Γ is the Gamma function [14]. We have no explanation so far of the origin of the phenomenological fit parameter G and we do not expect this estimate to hold for circular fibers with small values of the offset parameter.

A central goal in designing high-power DC fiber amplifiers and lasers is to increase the filling factor F, allowing one to scale down the required length for almost full pump absorption. Shortening the fiber length will mitigate against signal degradation through stimulated scattering [15] and offer a possibility of true single longitudinal mode operation. Recent developments in designing high-gain, short-length amplifiers in nonsilica glasses offers the possibility of scaling down the length of the fiber to centimeter lengths. However, most current DC fiber coupling geometries are not suitable for short-length devices due the their very poor coupling efficiencies. Scaling to short-length fibers requires that the relative core areas in the above formula be significantly increased. The very different aspect ratios of high-power incoherent diode bars and DC fiber

Manuscript received February 6, 2003; revised July 2, 2003. This work was supported by the Air Force Office of Scientific Research under Grant F49620-02-1-0380.

The authors are with the Arizona Center for Mathematical Sciences, Department of Mathematics, University of Arizona, Tucson AZ 85721 USA (e-mail: dima@acms.arizona.edu; jml@acms.arizona.edu).

Digital Object Identifier 10.1109/JQE.2003.818311

inner claddings requires complex intervening optics to fold the multiple linear emitter array outputs [16] to achieve approximately round beams for coupling into the near circular inner cladding.

In this paper, we propose to replace the almost circularly shaped inner cladding by a narrow slab waveguide that is mode-matched along the fast axis to the mode of the diode emitter(s). By butt-coupling the diode laser output to the slab waveguide, we ensure that most of the incoherent light from the emitter is guided in the slab. The doped core is placed next to the slab to ensure that the diode pump light is captured in the core.

We do not expect (1) to apply directly to this scenario as the design approach will require fine tuning of the slab and core refractive indices and geometries. From a practical point of view, we will want to align the diode bar at a small angle relative to the core axis. A key feature of the slab design is that the pump light is very efficiently and uniformly absorbed along the short length of core. This is in marked contrast to end-pump schemes where strong spatial nonuniformity of the pump absorption along the length of the fiber can enhance nonlinear instabilities. With the doped core being placed so close to the slab, it is strongly perturbed by the presence of the latter and, in principle, the generated signal within the core may leak back into the slab. The design must be such that only higher order signal modes leak into the slab while the fundamental, and possibly next higher order, modes are confined and amplified within the core.

For technological reasons, both the slab and core can be placed on some substrate. Also, the core can be protected with some small cladding. Such configurations should be more robust with respect to fluctuations of index of refraction and thickness of the slab. The analysis of such configurations will be the subject of future investigation. The aim of this paper is to show advantages of the slab pump of the fiber amplifiers. Therefore, we consider here the simplest configuration of the design of tapered slab delivery of the pump.

II. Slab-Core Geometry

In order to achieve high efficiency of absorption of the pump in a compact device, a significant part of the pump must be absorbed in a short distance of a few to tens of centimeters of the doped core. The fiber with local absorption rate of pump intensity $\alpha = 2$ cm^{-1} was used in [2]. Recently, fibers with $\alpha = 2$ cm^{-1} showed the record gain 5 dB/cm [17]. For example, a circularly symmetric inner cladding with small core in the center is a very poor geometry, with pump absorption efficiency $\eta < 4r/(\pi R)$ even for long-length fiber amplifiers [8], [9]. Here r and R are radii of the core and cladding, respectively. Very good mixing of partially coherent pump light can increase the efficiency to approach the fundamental limit (1) with $F = A_{\text{core}}/A_{\text{total}}$ as discussed in [10]–[12]..

A convenient approach to delivering a multimode pump source to some absorbing core is to facilitate the coupling of the pump into some cladding which supports multimode propagation. We therefore define the "cladding" as a transparent waveguide which supports propagation of the multimode pump. We do not assume that this cladding surrounds the core, as it does in the conventional DC fiber design [Fig. 1(a)]. Instead

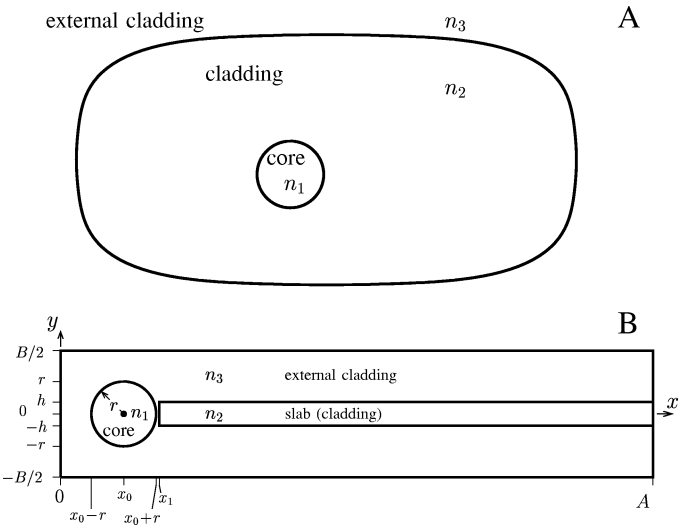

Fig. 1. (a) Cross section of the conventional DC fiber amplifier; the area of the core is much less than the area of the cladding; $n_1 > n_2 > n_3$. (b) Cross section of the slab-pumped fiber amplifier. For $h < r$, areas of the core and the cladding are comparable. The refractive index n_1 has no need to be greater than n_2.

a narrow transparent slab waveguide which is located close to the core, enables the coupled pump modes to penetrate the core [Fig. 1(b)]. In the conventional DC fiber geometries, the inner cladding diameter must be large enough to capture the pump light from an incoherent diode bar. Consequently, it must be much greater than the area of the core. Thus, if the pump source is wide (say, 100 μm), then at a fixed radius of the core (say, 4 μm), the area of the cross section of the cladding should be large (at least, greater than 800 μm^2, in the case of a rectangular cladding). Thus, the length of the amplifier must be much larger than in the case of the direct pump, at least by a factor of $F = A_{\text{core}}/A_{\text{total}} \approx 800/(16\pi) \approx 15$.

It should be noted that effective sources of pump light for the DC amplifiers, i.e., semiconductor lasers, produce partially coherent light. For realistic estimates we use data from the simulations described in [18]. The output beam of such a laser is highly coherent in one direction and has multimode structure in the orthogonal direction. Thus, the pump can be coupled into a thin strip, say, 1 μm $\times$ 100 μm, and the incoherent light can propagate in a waveguide of such a cross section.

If we can provide efficient coupling of the modes of such a narrow slab to the doped-core amplifier for a geometry as shown in Fig. 1(b), then the ratio $A_{\text{core}}/A_{\text{total}}$ can be increased to compare with conventional single-mode pump geometries; it can be an order of unity. Of course, such a simple estimate would become invalid as the thickness of the cladding becomes comparable to the wavelength of the pump. Even in this case we should expect a significant improvement in efficiency for coupling the pump into the active core relative to the case of conventional DC fiber.

Our goal is to confine the lowest order signal mode in the core while unwanted higher order signal modes leak into the slab. In the usual DC fiber, the core is designed to be single mode for signal propagation. In this case, the refractive index of the core is slightly higher than that of the inner cladding. Our situation here is fundamentally different. The core cannot be designed to

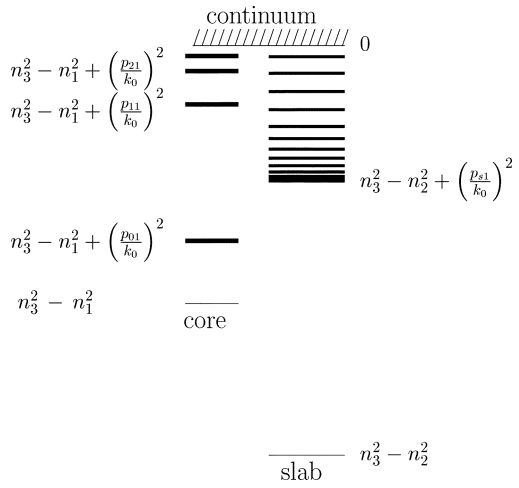

Fig. 2. Sketch of quasi-energies of the multimode core (left) and slab (right). Due to the "interaction" with the slab, the core becomes quasi-single-mode.

be strictly single mode for the signal as the nearby slab strongly perturbs the core, and such a mode could not be sustained along the core. Instead, we design the isolated core to be multimode at the signal wavelength and design the slab to capture the higher order signal modes. We also need to make the refractive index of the slab as large as possible so as to confine the maximal number of modes of the pump in the area with minimal cross section. An obvious question is how large this refractive index can be without enabling the lowest order signal mode to leak out of the core.

In order to understand this, we appeal to quantum mechanics. The confined field in a waveguide, as described within the paraxial approximation, is analogous to the wave function of a quantum particle confined in a two-dimensional potential. The negative of the square of the refractive index plays the role of the potential and the effective refractive index of a mode plays the role of the energy eigenvalue with associated eigenvector of the Hamiltonian. Fig. 2 provides a qualitative sketch of the quasi-energy levels of a composite system of core and slab. We neglect here, for simplicity, the interaction between the core and slab; this would correspond to a situation where the gap between the core and slab is relatively large. Assume that the ground state of the system is localized in the core. Generally the core has no need to be single mode at the signal wavelength. The criterion for the signal is that the quasi-energies of the remaining signal modes of the core be energetically higher than the majority of those of the slab. We will treat this situation quantitatively in the next section.

Qualitatively, Fig. 2 is valid for both the signal and pump. Inspection shows that the highest confined modes of the slab may be in resonance with excited modes of the core. This should ensure good coupling for these modes. The lowest confined modes of the slab are far from resonance and should show poor coupling to the core. The latter modes can be tuned into resonance by adiabatically tapering the slab along its length. Such tapering should eventually push the originally resonant higher slab modes into the continuum—however, these should already be efficiently absorbed by the core at the beginning of the slab.

We will now specify the modes of the slab that should be coupled to the input semiconductor laser and analyze the mode structure of the composite system core+slab in order to estimate the efficiency of the incoherent pump in such a system.

III. Modes of the Slab and Modes of the Fiber

This section provides an analysis of the mode structure of the composite slab-active core system. We will first present some standard waveguide analysis and derive some useful asymptotic design formulas. The latter facilitate the optimization of the composite core-slab structure over a wide multiparameter design space. We will establish the condition for quasi-single signal mode propagation more quantitatively. Again, for simplicity, we will assume that the core and slab are almost isolated. We formulate the condition where, on the one hand, the principal signal mode is confined to the core and, on the other hand, most other modes (signal and pump) penetrate into the slab. We will also assume small refractive index changes between the core, slab, and jacket so that a scalar assumption is appropriate.

If we assume weak coupling [7], [19], [20] of the signal and pump, we can consider the scalar Helmholtz equation

$$\Delta E + k^2(x,y)E = 0 \tag{2}$$

where the function $k^2(x,y) = \varepsilon(x,y) = n(x,y)^2 k_0^2$ describes distribution of the dielectric permitivity; the constant k_0 relates to the wavelength of the radiation, either pump or signal.

First, consider the case of an infinite slab. Let

$$n^2(x,y) = n^2(y) = \begin{cases} {n_2}^2, & |y| < h \\ {n_3}^2, & |y| < h \end{cases} \tag{3}$$

where n_2 is the index of refraction of the slab of thickness $2h$ and n_3 is the index of refraction of the external cladding (jacket). We reserve the notation n_1 for the index of refraction of the core (see Fig. 1). Looking for a propagating mode, we seek solutions of the form

$$E(x,y,z) = \sin(p_x x) f(y) \exp(i\beta z) \tag{4}$$

where β is the propagation constant [7]. Substituting (4) into (2), we obtain

$$f''(y) + \left(n^2(y){k_0}^2 - {p_x}^2 - \beta^2\right) f = 0 \tag{5}$$

where the prime denotes differentiation with respect to the y coordinate. The boundary condition $f(\infty) = 0$ can be satisfied if we represent the symmetrical solution of (5) as the combination of cosines and exponentials

$$f(y) = \begin{cases} \cos(p_y y), & |y| \le h \\ \cos(p_y h)\exp(q_y h)\exp\left(-q_y |y|\right), & |y| \ge h. \end{cases} \tag{6}$$

Using (3) and (5), we obtain the relations for the transverse wave numbers p_y and q_y as

$$-p_y^2 + n^2(y){k_0}^2 - {p_x}^2 - \beta^2 = 0 \tag{7}$$

$${q_y}^2 + n^2(y){k_0}^2 - {p_x}^2 - \beta^2 = 0. \tag{8}$$

Eliminating β^2 from these equations, we obtain a relation between p_y and q_y as follows:

$${q_y}^2 + n^2(y){k_0}^2 - p_x^2 - \beta^2 = 0. \tag{9}$$

Solving this equation with respect to q_y, we obtain

$$q_y{}^2 = \sqrt{(n_2{}^2 - n_3{}^2)\, k_0{}^2 - p_y{}^2}. \tag{10}$$

The condition of continuity of the function f and its derivative gives the equations

$$\cos(p_y h) = \cos(p_y h)\exp(q_y h)\exp(-q_y h) \tag{11}$$

$$-p_y \sin(p_y h) = -\, q_y \cos(p_y h)\exp(q_y h)\exp(-q_y h). \tag{12}$$

Combining (11) and (12), we obtain

$$p_y \tan(p_y h) = \sqrt{(n_2{}^2 - n_3{}^2)\, k_0{}^2 - p_y{}^2}. \tag{13}$$

The solution of (13) can be expressed in the following form:

$$p_y = \frac{P(V)}{h} = \frac{1}{h}\mathrm{slab}(V) \tag{14}$$

where $V = k_0 h\sqrt{n_2^2 - n_3^2}$ and the dimensionless function $g = \mathrm{slab}(V)$ is the lowest positive root of the dimensionless equation

$$\frac{g}{\cos(g)} = V. \tag{15}$$

The function slab is represented by the thick curve in Fig. 3(a). It has the following properties: expansion in small values of its argument

$$\mathrm{slab}(V) = V\left(1 - \frac{1}{2}V^2 + \frac{13}{24}V^4 + O(V^6)\right). \tag{16}$$

An asymptotic solution at large value of the argument is

$$\mathrm{slab}(V) = \frac{(\frac{\pi}{2})V}{V + 1 + O\left(\frac{1}{V^2}\right)}. \tag{17}$$

Approximation with rational functions gives

$$\begin{aligned}\mathrm{slab}(V) = {} & (14.504\,766(3.651\,515\,7 + V) \\ & \times (0.314\,498\,1 + 0.592\,445V + V^2) \\ & \times (0.160\,580\,04 + 0.756\,039\,24V + V^2)t^{16} \\ & - 3.262\,737t^9 + 1.276\,687\,4t^7 - 0.612\,850\,1t^5 \\ & -0.646\,710\,1t^3 + 1.570\,796\,5)\, Vt + \delta\end{aligned}$$

where

$$t = \frac{1}{1+V}; \quad |\delta| < 2\times 10^{-7}, \quad V|\delta| < 2\times 10^{-7}$$
$$\text{at} \quad 0 < V < \infty. \tag{18}$$

In the literature [18], [19], the normalized frequency

$$b(V) = 1 - \frac{P(V)^2}{V^2} \tag{19}$$

is used to characterize waveguides. For the slab, the function $b(V)$ is presented in Fig. 3(b) as a thick curve.

The corresponding effective decay rate q_y of the function f given by (6) can be expressed in terms of $P(V)$ as follows:

$$q_y(V) = \frac{Q(V)}{h} = \frac{\sqrt{V^2 - \mathrm{slab}(V)^2}}{h} = \frac{V\sqrt{b(V)}}{h}. \tag{20}$$

For the slab, the function $Q(V)$ is represented by the thick curve in Fig. 3(c). This function increases monotonically and, at large values of V, becomes a linear function of its argument.

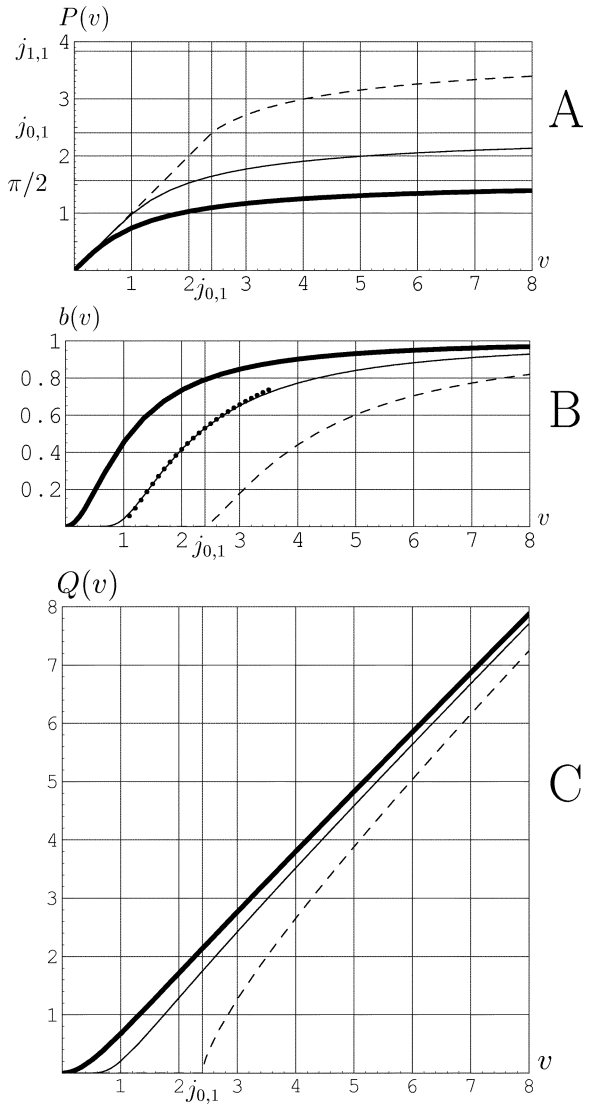

Fig. 3. Functions $P(V)$, $b(V)$, and $Q(V)$ for the principal mode of the slab (thick curves) and for the first two modes of the fiber (thin curves for mode 0, 1, and dashed curves for mode 1,1). In the graph of $b(V)$ the dotted curve represents the fit (28) valid at $1.5 < V < 2.5$.

The above approximations enable us to effectively evaluate all of the parameters in (6).

A similar analysis can be applied to the case with circular symmetry. Here, we are interested mainly in the principal mode and, possibly, the next higher order mode of the active core, because other modes are expected to be strongly mixed with modes of the slab. In the simplest case, the distribution of the dielectric permitivity can be described with the step function

$$n^2(x,y) = \begin{cases} n_1^2, & x^2 + y^2 < r \\ n_2^2, & x^2 + y^2 > r. \end{cases} \tag{21}$$

(We reserve the notation n_2 for the refractive index of the slab). Using polar coordinates, the principal mode can be expressed in terms of the Bessel functions J and K as

$$\psi_{0,1}(x,y) = \begin{cases} J_0(p\rho), & \rho \le r \\ \frac{J_0(pr)}{K_0(qr)} K_0(q\rho), & \rho \ge r \end{cases} \tag{22}$$

where the transverse wavenumbers p and q are solutions of the equations

$$J_0(qr)qK_1(qr)=K_0(qr)pJ_1(pr),\quad q^2+p^2=k_0^2\left(n_1^2-n_3^2\right). \tag{23}$$

The solutions of (23) can be expressed in terms of dimensionless functions of $V=k_0h\sqrt{n_1^2-n_3^2}$ [7], [19], [20], as in the case of the slab $p=(P(V))/r$, $q=(Q(V))/r$, where

$$P=V\sqrt{1-b(V)},\quad Q=V\sqrt{b(V)}=\sqrt{V^2-P^2}. \tag{24}$$

For the case of the core, the functions P,b,Q are presented in Fig. 2(a)-(c) with thin curves. For the principal mode of the core, the function $b_{0,1}(V)$ has the following properties:

$$0<b_{0,1}(V)<1,\quad {b_{0,1}}'(V)>0 \tag{25}$$

$$b_{0,1}(V)=\frac{4}{V^2}\exp\left(-\frac{4}{V^2}-2\gamma+\frac{1}{2}+O(V^2)\right),\quad \text{at } V\ll 1 \tag{26}$$

$$b_{0,1}(V)=\frac{V^2}{V^2+j_{0,1}+O\left(\frac{1}{V}\right)},\quad \text{at } V\gg 1 \tag{27}$$

where $\gamma\approx 0.577\,215\,664\,9$ is the Euler's constant [14] and $j_{0,1}\approx 2.404\,825\,557\,7$ is the first zero of the Bessel function J_0. It should be noted that the following rational approximation [20] exists for the function b for the principal mode (0,1) of the core:

$$b_{0,1}(V)=\tilde{b}(V)+\delta$$

where

$$\tilde{b}(V)=\left(1.1428-\frac{.996}{V}\right)^2 \text{ and } |\delta|<0.002 \quad \text{at}\quad 1.5\le V\le 2.5. \tag{28}$$

The function $b_{0,1}(V)$ is shown in Fig. 3(b) by a dotted line; it practically coincides with the exact solution within the range $1.5\le V\le 2.5$. However, for the case of the amplifier, there is no reason to limit the consideration to this interval. Therefore we suggest the following approximation:

$$\begin{aligned}b_{0,1}(V)=&\frac{\exp\left(\frac{-4}{V^2}\right)}{(0.25+V)^{10}}\\&\times\left(V^{10}+2.499\,89V^9+1.035\,98V^8+8.841\,02V^7\right.\\&-6.212\,64V^6+19.099\,16V^5-15.1575V^4\\&+11.557\,96V^3+1.173\,32V^2-4.295\,57V\\&\left.+1.2809\right)+\delta\end{aligned}$$

where

$$|\delta|<6\times 10^{-7} \text{ at } 0\le V\le\infty. \tag{29}$$

A similar analysis can be done for the first excited mode:

$$\psi_{1,1}(x,y)=\begin{cases}J_1(p\rho), & \rho\le r\\ \frac{J_1(pr)}{K_1(qr)}K_1(q\rho), & \rho\ge r.\end{cases} \tag{30}$$

It happens to be easier to fit function $P_{1,1}(V)$ as shown in (31) at the bottom of the page and reconstruct $b_{1,1}$ and $Q_{1,1}$ from (19) and (24).

The advantages of fits (18), (29), and (31) are not only the high precision and extended region of validity of the approximation in comparison to (28), but also the smoothness: these fits can be differentiated several times, and the results still approximate the derivatives of the initial functions. To our knowledge, no similar approximation was reported before, and these fits can be a useful design tool.

The effective propagation constants of the slab and the core should be close for good coupling of the pump light. For example, using values

$$\begin{aligned}n_1&=1.56\\n_2&=1.57\\n_3&=1.55\\r&=4.3\,\mu\\h&=0.5\,\mu\\k_0&=\frac{2\pi}{(0.98\,\mu)}\end{aligned} \tag{32}$$

for the slab, we obtain

$$\begin{aligned}V_{\text{slab}}&=k_0h\sqrt{n_2^2-n_3^2}=0.800\,785\\P_{\text{slab}}&=\text{slab}(V_{\text{slab}})=0.641\,560\\q_{\text{slab}}&=\frac{\sqrt{{V_{\text{slab}}}^2-{P_{\text{slab}}}^2}}{h}=0.958\,453\,\mu^{-1}\\\beta_{\text{slab}}&=\sqrt{n_3^2k_0^2+{q_{\text{slab}}}^2}=9.983\,80\,\mu^{-1}.\end{aligned} \tag{33}$$

For the same values (32) for the core we have $V_{\text{core}}=k_0r\sqrt{n_1^2-n_3^2}=4.861\,860$, then we use fit (29) to get $b_{0,1}=b_{0,1}(V_{\text{core}})=\sqrt{n_3^2k_0^2+q_{\text{slab}}^2}=0.833\,490$ for the principal mode and the fit (31) to get $P_{1,1}=P_{1,1}(V_{\text{core}})=3.134\,63$ for the first excited mode. It should be noted that (24) holds for both slab and fiber, and (20) can be used for the fiber if we substitute $h\to r$. Using these equations, we obtain

$$\begin{aligned}q_{0,1}&=\frac{V_{\text{core}}\sqrt{b_{0,1}}}{r}=1.032\,25\,\mu^{-1}\\\beta_{0,1}&=\sqrt{n_3^2k_0^2+{q_{0,1}}^2}=9.991\,16\,\mu^{-1}\\q_{0,1}&=\frac{\sqrt{{V_{\text{core}}}^2-{P_{0,1}}^2}}{r}=0.864\,28\,\mu^{-1}\\\beta_{1,1}&=\sqrt{n_3^2k_0^2+{q_{1,1}}^2}=9.975\,20\,\mu^{-1}.\end{aligned} \tag{34}$$

$$\begin{aligned}P_{1,1}(V)&=r\,p_{1,1}\\&=\frac{j_{0,1}+45.099\,71t+66.593t^2+63.805\,26t^3+47.540\,988t^4+12.858\,587t^5+4.533\,426t^6}{1+18.753\,84t+27.308\,54t^2+19.961\,799\,7t^3+13.593\,472t^4+3.355\,74t^5+1.183\,136\,3t^6}\end{aligned}$$

where

$$t=\sqrt{V-j_{0,1}},\quad |\delta|<10^{-7}\quad \text{at}\quad j_{0,1}\le V<\infty \tag{31}$$

The closeness of the effective propagation constants $\beta_{\rm slab}$ to $\beta_{0,1}$ and $\beta_{1,1}$ allows good coupling of the pump light between the slab and core. We anticipate that the configuration [Fig. 1(b)] with values of the parameters (32) should realize very effective pumping of the core.

The example above is not the only configuration that ensures good pump absorption while maintaining quasi-single-mode propagation for the signal. Generally, a quasi-single-mode core corresponds to the condition $\beta_{0,1} > \beta_{\rm slab} > \beta_{1,1}$. We can define functions $q_y(n_{\rm in}, n_{\rm out})$ and $q_{m,j}(n_{\rm in}, n_{\rm out})$ as values of parameter q for the principal mode of the slab and that for the mode number j of the core with angular momentum m. Here $n_{\rm in}$ and $n_{\rm out}$ are indices of refraction of the inner region (n_1 for the core and n_2 for the slab) and for the outer region (n_3 in both cases above), respectively. Then the condition for a quasi-single-mode core can be rewritten as

$$q_{0,1}(n_1, n_3) > q_{\rm slab}(n_2, n_3) > q_{1,1}(n_1, n_3). \qquad (35)$$

This condition is satisfied for values of q given in (33) and (34). The condition (35) is represented graphically in Fig. 4 for the case $r = 4.3$ μm and varying thicknesses $2h$ (0.4, 1, and 2 μm) of the slab. The example design above corresponds to the point (0.02, 0.01) in the second graph, marked with a circle. We note from Fig. 4 that the narrower the slab, the more robust the design to variations in refractive index.

The dependence of the field of the pump in the x direction in the slab should slightly decrease the propagation constant, providing almost exact resonance with the core, as shown in Fig. 2. This can be seen from numerical analysis of the mode structure of the waveguide which includes both core and slab.

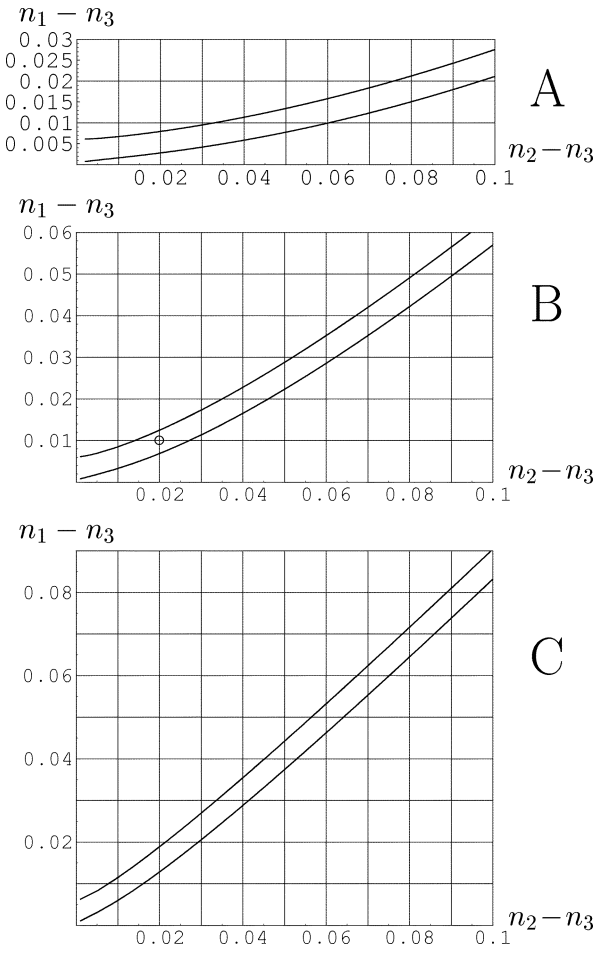

Fig. 4. Key design relations for quasi-single-mode fiber: upper and lower boundaries of $n_1 - n_2$ as solutions of (35) versus $n_2 - n_3$ at (a) $2h = 0.4$ μm^{-1}, (b) $2h = 1$ μm^{-1}, and (c) $2h = 2$ μm^{-1}. Parameters used in (32)–(34) are represented by the circle in Fig. 4(b).

IV. Calculation of Modes: the Numerical Approach and the Decoherence Approximation

From the consideration of isolated core and isolated slab in the previous sections, we made some predictions and recommendations about the slab pump of the fiber amplifier. While the slab is thin, we can expect small interaction between modes localized in slab and modes localized in the core. In this section, we analyze the modes of the pump in the waveguide taking into account both core and slab.

In the decoherence approximation [11], the efficiency of absorption of the mode Ψ_m in the core can be expressed as follow:

$$\eta_m = 1 - \exp(-F_m \alpha z) \qquad (36)$$

where

$$F_m = \int\limits_{(x-x_0)^2+y^2<r^2} \Psi_m(x,y)^2 dx\, dy \qquad (37)$$

is the filling factor of the mth mode. (Ψ_m is normalized, $\int \Psi(x,y)^2 dxdy = 1$). Here, all the modes Ψ_m of the waveguide are calculated in the absence of absorption. Such modes are solutions of (2). For the case of Fig. 1(b), we approximate the dependence of the index of refraction on the coordinates in the following way:

$$n(x,y) = \begin{cases} n_1 & \text{at} \quad (x-x_0)^2 + (y-y_0)^2 < r^2, & x < x_0 \\ n_3 & \text{at} \quad (x-x_0)^2 + (y-y_0)^2 > r^2, & x < x_0 \\ n_2 & \text{at} \quad |y| < h, & x > x_0 \\ n_3 & \text{at} \quad |y| > h, & x > x_0 \end{cases} \qquad (38)$$

Using the spectral method [11], the operator $\Delta - k_0^2 n^2$ was diagonalized in the momentum representation for values of parameters specified in (32). The core was located at point $x_0 = 8$ μm, $y_0 = 0$ while the coordinates of the left end of the slab are $x_1 = 12.5$ μm, $y_1 = 0$. We use a 1024×128 grid, grid size $d_x = 0.11$ μm, $d_y = 0.15$ μm corresponds to $A = 112.64$ μm, $B = 19.20$ μm in Fig. 1.

Harmonics with a transversal wavenumber less than $K_{\max} = 3$ μm^{-1} were taken into account. The amplitude of the 40 resulting modes is shown in Fig. 5. Other modes correspond to unbound states of the slab and fill the box $A \times B$, practically avoiding both core and slab. The filling factor F_m is shown in Fig. 6 versus m. Roughly speaking, the initial power of excitation of each mode should be proportional to the overlap of the

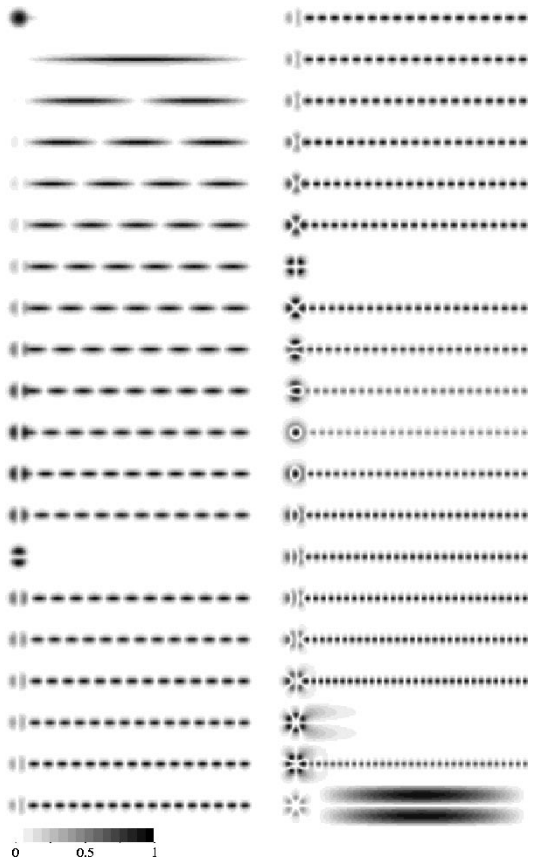

Fig. 5. Distribution of amplitude of the first 40 modes of the pump.

square of the mode with the slab transversal mode. This overlap can be expressed as follows:

$$C_m = \int_{x_1}^{A} \left(\int_{-\frac{B}{2}}^{\frac{B}{2}} \Psi_m(x,y) f(y) dy \right)^2 dx \qquad (39)$$

where f_y is the normalized solution for the slab. These coefficients are plotted in Fig. 6 with circles.

The overlapping of modes with the core shows a smooth trend. The lowest modes of the slab are almost uncoupled from the core and there exist some resonances. For the highest modes, the coupling is strong and these are rapidly absorbed. We could expect this from inspection of Fig. 2. The modes in the slab part are almost sinusoidal, and coupling with the core is determined by the transversal wavenumber of this sinusoid. With adiabatic tapering of the slab, the wavenumber of the remaining uncoupled modes should increase and at some length of propagation the wavenumber of each mode tunes into resonance with the core. At this length, this mode will be efficiently absorbed. As a result, the core consumes all modes of the tapered slab one by one, as they come into the resonance. This conclusion is verified below in the Section VII with numerical simulations. However, for the simulations, we need to specify the field of the pump.

V. Incoherent Diode Pump Field

For the numerical analysis, we use simulations with an input pump field as described in [18]. Fig. 7(a) shows the time-averaged near-field intensity of the diode-pump along the slow (x) axis. The result is the average of 5000 realizations. Most of the field is located within the lateral rectangle box of width 100 μm. Fig. 7(b) shows the lateral mode content of the incoherent diode emitter. This is represented as the squared modulus of the Fourier components. We conclude that about 32 Fourier harmonics are excited in the diode pump field.

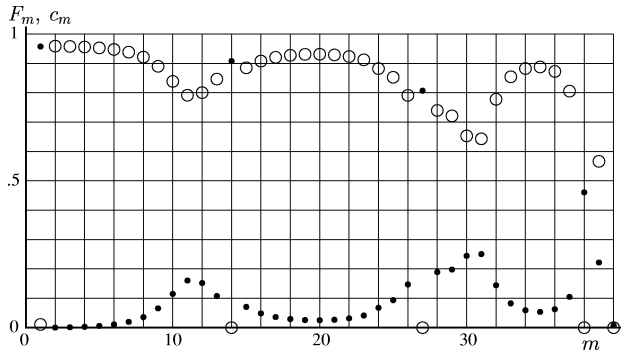

Fig. 6. Filling factor F_m (dots) given by (37) and the overlap c_m with the slab (circles) given by (39) versus mode number m for the conditions expressed in (32).

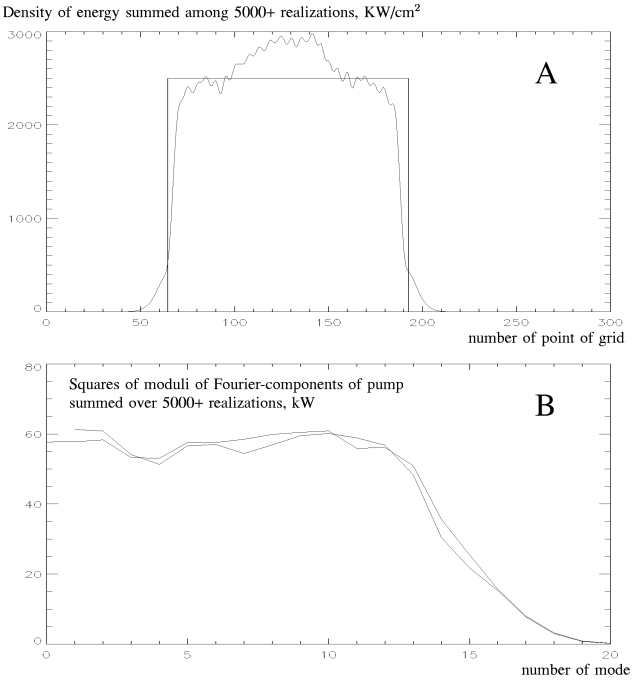

Fig. 7. (a) Spatial distribution of the output power of a broad area semiconductor laser summed over several thousand realizations as simulated in [18]. (b) Distribution of the output power of the semiconductor laser among the Fourier harmonics, calculated over the significant part of the spatial domain enclosed by the rectangle in the previous graph.

Returning to Fig. 5, we see, that the 39th mode has about 32 nodes in the slab part. Thus, we can assume that first $M = 40$ modes are excited with relative power $c_m = P_0/40$ where P_0 is initial power of the pump. Then the decoherence approximation [3] gives a qualitative estimate of the pump absorption efficiency in the slab-core geometry:

$$\eta = \sum_{m=1}^{M} c_m \eta_m. \qquad (40)$$

This equation should overestimate the efficiency because of antisymmetric modes which show good coupling with the core but do not enter the slab and therefore are not excited at all. The estimate (40) can be improved using

$$c_m = P_0 \frac{C_m}{\sum_n C_n}$$

(instead of $c_m = P_0/M$ mentioned above). Such an updated estimate gives almost the same result for the efficiency of the pump absorption, so we do not discuss it here. These estimates are confirmed with direct simulations described in the following sections.

VI. Beam Propagation Method

As the verification of the analysis above, we carried out a beam propagation study of the slab device. All of the field is assumed to be localized within the rectangle $A \times B$ and symmetric with respect to $y \to -y$. The modes of this rectangle were used instead of the complex exponentials in the standard beam propagation method (BPM) scheme [21]. The mode expansion is in the terms of discrete sine-and staggered cosine transforms.

Examples of the resulting pump absorption efficiency are plotted in Fig. 8. The reference solid curves are the same for both cases. The upper solid curves correspond to the estimate (40); the lower correspond to the estimate [11, eq. (11)] for the case of a circular cladding of radius 10 μm. All simulated curves lie between these two limiting cases. The thin solid curves in case (a) represent 10 simulations with BPM using 10 realistic initial conditions using the approach described in [18], and the bars show their mean-square deviation. These simulations were done with a 256×64 grid with $d_x = 0.44$ μm, $d_y = 0.2$ μm, $d_z = 1$ μm, $r_0 = 4.3$ μm, $x_0 = 8$ μm, $x_1 = 8$ μm, $h = 05.$ μm, $n_1 = 1.56$, $n_2 = 1.57$, $n_3 = 1.55$, $\alpha = 2$ cm^{-1}.

The simulations were repeated for various values of pump absorption rate α. The pump absorption efficiency is plotted in Fig. 8(b) versus dimensionless parameter $Z = \alpha z$. We see that, for reasonable values $\alpha \approx 10$ cm^{-1} or less, the scaling discussed in [10] is reproduced: the effective absorption rate is proportional to the local absorption rate α. Significant deviation appears only at an unrealistic linear absorption rate $\alpha \approx 40$ cm^{-1}. Thus, we expect the scaling to be valid for all reasonable values of α.

VII. Tapered Slab

Tapering of the slab should significantly improve the performance of the device. This follows from the qualitative considerations in Section II, as well as from the analysis of modes in Section IV. In this section, we check this conclusion with numerical simulations.

Assume that the slab occupies the region from x_1 to $x_2 = x_2(z)$ where $x_2(z)$ assumes the following functional form:

$$x_2(z) = \mathrm{Max}\left(x_1(z), 1 - \frac{z}{2\ \mathrm{cm}} A\right). \tag{41}$$

This function allows a linear tapering with a possible cut-off before the end of the device. We specialize here to a 2-cm-long device. The coordinate $x_2(z)$ is plotted in Fig. 9 as the linearly decreasing line from left to right. (Actually, we plot the dimensionless ratio $x_2(z)/A$ to keep the same scale for all graphs.)

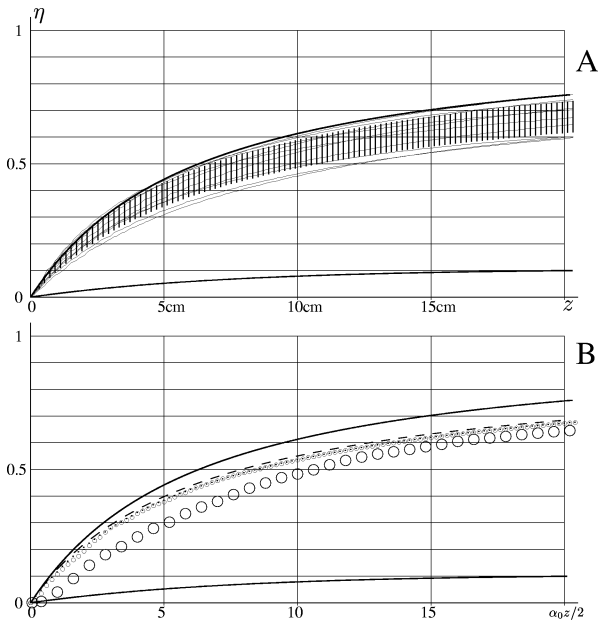

Fig. 8. Efficiency of absorption of the pump in various cases. The upper thick solid curve in both cases (a), (b) represents the estimate by (40), and the lower solid curve represents the case of circular cladding with centered core. Other curves represent the results of the simulations with BPM. (a) Ten realizations (thin curves) and the mean-square deviation (bars) for $\alpha = 2$ cm^{-1}. (b) Mean value among 10 realizations for $\alpha = 1$ cm^{-1} (dashed curve), $\alpha = 2$ cm^{-1} (dotted curve), $\alpha = 10$ cm^{-1} (small circles), and $\alpha = 40$ cm^{-1} (large circles).

We use the same 10 realizations of the pump as in the previous section. The solid curve shows the pump absorption efficiency over the 2-cm length of the core with $\alpha = 10$ cm^{-1}. We predict greater than 90% absorption over 2 cm. Without tapering, the absorption efficiency would be given by the dashed curve. The lowest (open circles) curve corresponds to the case where the slab is removed and the cladding (all the $A \times B$ domain) is pumped directly. This would corespond to a double clad fiber having a rectangular inner cladding with an offest core.

In all the simulations, the initial condition $E(x, y, 0)$ was the same. The initial field was multiplied by the phase factor $\exp(-i0.2\ \mu\mathrm{m}^{-1}x)$, corresponding to an inclination of the pump with respect the core axis by an angle $0.2\ \mu\mathrm{m}^{-1}/k_0 n_2 \approx 1.3^\circ$ toward the core.

Fig. 9 shows the significant improvement of the pump absorption efficiency due to the tapering of the slab. We should also stress that the tapered slab allows an almost constant pump intensity along the core. This is important to minimize signal noise and avoid spatial hole burning.

At the appropriate tapering, most of pump is absorbed in the core, as in the simulations above. However, a few percent of the pump becomes unbounded, as this part of pump escapes from the waveguide. Due to the multiple reflections at the tapered part of the slab, some part of the pump could be even scattered back and destabilize the source of pump. However, at the small angle of tapering (less than 1% in the example above), and the reflection coefficient of order of 5% for the rays which are almost orthogonal to the optical axis, the backscattered part of the pump is exponentially small and does not need to be taken into

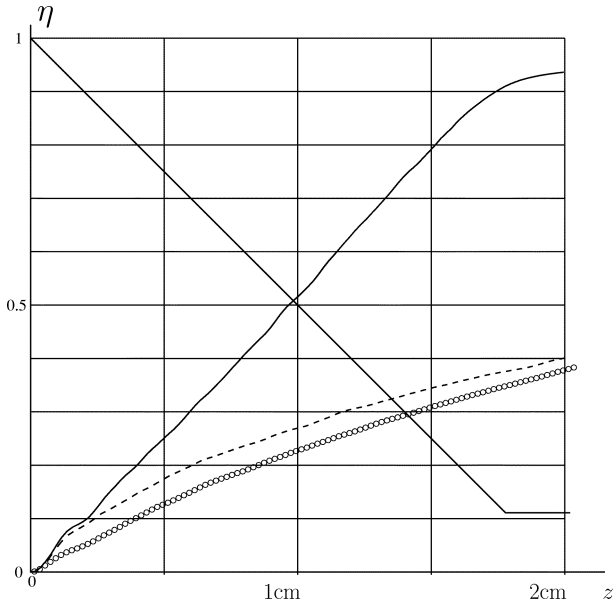

Fig. 9. Efficiency of absorption of the pump versus length of tapered amplifier (upper solid curve). The coordinate $x_2(z)/A$ of the tapered side of this amplifier is given by (41) (descending segmented curve). For comparison, we also present the efficiency for the case without tapering (dashed curve) and the efficiency for the case of a rectangular clad (circles).

account. Most of the pump is used in the core, and the rest is scattered forward at small angles.

VIII. Other Geometries and Power Scaling

The configuration shown in Fig. 1(b) is just one possible realization of a slab pump geometry. It is particularly convenient for numerical simulation and verification of the overall design concepts put forth in this paper. This design can be scaled to accommodate a diode bar pump, rather than a single emitter. The device length should be scaled appropriately. In addition, two diode bars can pump slabs on both sides of the central doped core. Fig. 10 shows a possible slab-pump geometry for power scaling. The second slab, placed symmetrically on the other side of the core, has the added advantage that it effectively cancels out the antisymmetric $(y \rightarrow -y)$ higher order modes of the signal. This would more strongly favor propagation of the fundamental signal mode in the core.

In this geometry, the core and slabs can be placed on the same lower index substrate. One could envisage a cascaded slab-pump arrangement along the length of a device where each diode bar is offset at an angle to the core axis and coupled into its own angled slab waveguide. Efficient cooling should be possible by bringing the coolant itself closer to the active core and ensuring that the coolant refractive index satisfies the refractive index design criteria developed earlier. In other words, the coolant itself would act as a top cladding for the device.

The slab pump delivery could be even more robust if we substitute the naked core in Figs. 1 and 10 to a fiber with narrow "chaotic" cladding. Fibers with various noncircular claddings were fabricated recently [22]–[24]. Such fibers can be coupled to a tapered waveguide in analogy with a side-pumping coupler

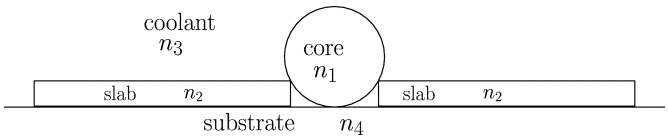

Fig. 10. Cross section of a realistic design of the slab-pumped fiber amplifier: two-slab geometry.

[25]. The appropriate relation between length of tapering and the effective absorption rate of pump [26] allow effective and compact devices.

IX. Conclusion

We propose a new geometry of double-clad amplifiers/lasers where the conventional cladding is replaced by a tapered slab waveguide. The core is designed to be quasi-single mode for the signal. Design criteria and formulas are provided that depend explicitly on the refractive indices of the core, slab, and cladding. Our study is based on the decoherence approximation [11] and modal and numerical analysis. We demonstrate that the incoherent diode pump absorption efficiency can be significantly improved by tapering the slab. Assuming a local absorption rate $\alpha = 10\ \text{cm}^{-1}$ (for highly doped phosphate glass) and an amplifier length of 2 cm, the pump absorption efficiency can be of the order of 94%.

Acknowledgment

The authors are grateful to M. Kolesik, R. Indik, A. Mafi, M. Mansuripur, V. Temyanko, N. Peyghambarian, and other colleagues at the Arizona Center for Mathematical Sciences and the Optical Science Center of the University of Arizona for the stimulating discussions.

References

[1] B. Rossi, "Commercial fiber lasers take on industrial markets," *Laser Focus World*, vol. 33, no. 5, pp. 143–149, 1997.
[2] Y. C. Yan, A. J. Faber, H. de Waal, P. G. Kik, and A. Polman, "Erbium-doped phosphate glass waveguide on silicon with 4.1 dB/cm gain at 1.535 micron," *Appl. Phys. Lett.*, vol. 71, no. 20, pp. 2922–2924, 1997.
[3] B. C. Hwang, S. Jiang, T. Luo, J. Watson, S. Honkanen, Y. Hu, F. Smektala, J. Lucas, and N. Peyghambarian, "Erbium-doped phosphate glass fiber amplifiers with gain per unit length of 2.1 dB/cm," *Electron. Lett.*, vol. 35, no. 12, pp. 1007–1009, 1999.
[4] V. Dominic, S. MacCormack, R. Waarts, S. Bicknese, R. Dohle, E. Wolak, P. S. Yeh, and E. Zucker, "110 W power fiber laser," *Electron. Lett.*, vol. 35, pp. 1158–1160, 1999.
[5] E. M. Dianov, A. V. Belov, I. A. Bufetov, V. N. Protopopov, A. N. Gur'yanov, D. D. Gusovskii, and S. V. Kobis, "High-power single-mode neodymium fiber laser," *Quantum Electron.*, vol. 27, no. 1, pp. 1–2, 1997.
[6] J. Q. Xi, M. Prabhu, J. R. Lu, K. Ueda, and D. Xing, "Efficient double-clad thulium-doped fiber laser with a ring cavity," *Appl. Opt.*, vol. 40, no. 12, pp. 1983–1988, 2001.
[7] A. W. Snyder and J. D. Love, *Optical Waveguide Theory*. New York: Chapman & Hall, 1983.
[8] S. Bedö, W. Lüthy, and H. P. Weber, "The effective absorption coefficient in double-clad fibers," *Opt. Commun.*, vol. 99, no. 5–6, pp. 331–335, 1993.
[9] D. Kouznetsov, J. V. Moloney, and E. M. Wright, "Efficiency of pump absorption in double-clad fiber amplifiers. 1. Fiber with circular symmetry," *J. Opt. Soc. Amer. B*, vol. 18, no. 6, pp. 743–749, 2001.
[10] D. Kouznetsov and J. V. Moloney, "Efficiency of pump absorption in double-clad fiber amplifiers. 2. Broken circular symmetry," *J. Opt. Soc. Amer. B*, vol. 19, no. 6, pp. 1259–1263, 2002.

[11] ——, "Efficiency of pump absorption in double-clad fiber amplifiers. 3. Calculation of modes," *J. Opt. Soc. Amer. B*, vol. 19, no. 6, pp. 1304–1309, 2002.
[12] P. Leprox, S. Fevrier, V. Doya, P. Roy, and D. Pagnoux, "Modeling and optimization of double-clad fiber amplifiers using chaotic propagation of the pump," *Opt. Fiber Technol.*, vol. 7, no. 4, pp. 324–339, 2001.
[13] A. Liu and K. Ueda, "The absorption characteristics of circular, offset, and rectangular double-clad fibers," *Opt. Commun.*, vol. 132, pp. 511–518, 1996.
[14] M. Abramovitz and I. A. Stegun, *Handbook for Mathematical Functions*. Boulder, CO: Nat. Bureau of Standards, 1964.
[15] G. S. He, "Optical phase conjugation: principles, techniques and applications," *Prog. Quantum Electron.*, vol. 26, pp. 131–191, 2002.
[16] W. A. Clarkson and D. C. Hanna, "Two-mirror beam-shaping technique for high-power diode bars," *Opt. Lett.*, vol. 21, no. 6, pp. 375–577, 1996.
[17] Y. Hu, S. Jiang, T. Luo, K. Seneschal, M. Morrell, F. Smektala, S. Honkanen, J. Lucas, and N. Peyghambarian, "Performance of high-concentration Er^{3+} – Yb^{3+}-codoped fiber amplifiers," *IEEE Photon. Technol. Lett.*, vol. 13, pp. 657–659, July 2001.
[18] J. V. Moloney, R. A. Indik, J. Hader, and S. W. Koch, "Modeling semiconductor amplifiers and lasers: from microscopic physics to device simulation," *J. Opt. Soc. Amer. B*, vol. 16, no. 11, pp. 2023–2029, 1999.
[19] F. Tosco, *Fiber Optics Communications Handbook* London, U.K., 1990, Tab Professional and Reference Handbooks.
[20] G. P. Agrawal, *Fiber-Optics Communication Systems*. London, U.K.: Prentice-Hall, 1993.
[21] A. Newel and J. V. Moloney, *Nonlinear Optics*. Redwood City, CA: Addison-Wesley, 1992.
[22] R. Renner, M. Kehrli, W. Lüthy, and H. P. Weber, "Manufacturing of a D-shaped fiber," *Laser Physics*, vol. 13, no. 2, pp. 232–233, 2003.
[23] P. Leproux, V. Doya, P. Roy, D. Pagnoux, F. Mortessagne, and O. Legrande, "Experimental study of pump power absorption along rare-earth-doped double clad optical fibres," *Opt. Commun.*, vol. 218, no. 4–6, pp. 249–254, 2003.
[24] D. Young and C. Roychoudhuri, "Results and comparison of a cladding pumped fiber amplifier simulator using a decagon-shaped fiber," *Opt. Express*, vol. 11, no. 7, pp. 830–837, 2003.
[25] J. Xu, J.-H. Lu, G. Kumar, J. R. Lu, and K. Ueda, "A non-fused fiber coupler for side-pumping of double-clad fiber lasers," *Opt. Commun.*, vol. 220, no. 4-6, pp. 389–395, 2003.
[26] D. Kouznetsov and J. Moloney, "Slab delivery of pump light to double-clad fiber amplifiers: An analytic approach," *IEEE J. Quantum Electron.*, submitted for publication.

Dmitrii Kouznetsov received the Ph.D. degree from the Lebedev Physics Institute, Moscow, Russia, in 1988.

While at the Lebedev Physics Institute, he invented the method of the active image formation, in collaboration with T. I. Kuznetsova (1985) and had formulated and proved the original theorems about the quantum stability of the optical soliton (1991–1992). In 1992, he joined the Mexican National autonomous University (UNAM, Mexico), until its crash in 1999. There he had proved several original theorems about the quantum noise of the nonlinear amplifier, in collaboration with D. Rohrlich (1993–1995), and suggested the method of random wavevectors in simulations of correlated random processes with wide spectra (1995–1999). Since 2000, he has been with the Arizona Center for Mathematical Sciences, University of Arizona, Tucson.

Jerome V. Moloney received the B.Sc. degree from University College, Cork, Ireland, in 1970 and the Ph.D. degree from the University of Western Ontario, ON, Canada, in 1977.

He is the Director of the Arizona Center for Mathematical Sciences, University of Arizona, Tucson, Professor of Mathematics, Professor of Optical Sciences, and Visiting Professor of Computational Physics, University College Cork. He has been a Professor with the Department of Mathematics and Optical Sciences Center, University of Arizona, since 1985. He has been with the Optical Sciences Center, University of Arizona, since 1979, in several capacities: Research Associate Professor (1984–1985), Research Assistant Professor (1981–1984), and Research Associate (1979–1981). He was a Reader in Physics (1984–1990), Heriot-Watt University, Edinburgh, U.K., and a Research Associate (1977–1979), Universitate Bielefeld, West Germany. His research includes: mathematical modeling and simulation of photonics systems including semiconductor lasers, fiber lasers, and photonic Bragg and photonic crystal fibers; fundamental theory of semiconductor lasers including microscopic physics; modeling high-power femtosecond atmospheric light strings; nonlinear theory of partial differential equations and chaos synchronizations in extended complex spatiotemporal interacting systems; sophisticated algorithm development for large-scale computational photonics systems simulations including adaptive mesh refinement and parallelization distributed and shared memory supercomputer platforms.

Prof. Moloney is involved with the National Research Council, the Naval Studies Board, and the Workshop on Mathematics. He is a member of Mathematics in Material Sciences and the Society for Industrial and Applied Mathematics. He is a member of the Organizing Committee, University of Minnesota, Institute of Mathematics and Its Applications, and Organizer of the Workshop on Nonlinear Optical Materials.